



OPEN ACCESS

EDITED BY

Leonardo Bernasconi,
University of Pittsburgh, United States

REVIEWED BY

De Nyago Tafen,
National Energy Technology Laboratory (DOE),
United States
Christian Tantardini,
UiT The Arctic University of Norway, Norway

*CORRESPONDENCE

Evangelos Miliordos,
✉ emiliord@auburn.edu

†PRESENT ADDRESS

Emily E. Claveau,
Department of Chemistry, Michigan State
University, East Lansing, United States

RECEIVED 09 October 2024

ACCEPTED 11 November 2024

PUBLISHED 11 December 2024

CITATION

Claveau EE and Miliordos E (2024) Electronic structure of metal oxide dications with ammonia ligands and their reactivity towards the selective conversion of methane to methanol.
Front. Chem. 12:1508515.
doi: 10.3389/fchem.2024.1508515

COPYRIGHT

© 2024 Claveau and Miliordos. This is an open-access article distributed under the terms of the [Creative Commons Attribution License \(CC BY\)](https://creativecommons.org/licenses/by/4.0/). The use, distribution or reproduction in other forums is permitted, provided the original author(s) and the copyright owner(s) are credited and that the original publication in this journal is cited, in accordance with accepted academic practice. No use, distribution or reproduction is permitted which does not comply with these terms.

Electronic structure of metal oxide dications with ammonia ligands and their reactivity towards the selective conversion of methane to methanol

Emily E. Claveau[†] and Evangelos Miliordos^{*†}

Department of Chemistry and Biochemistry, Auburn University, Auburn, AL, United States

High-level quantum chemical calculations are performed for the $(\text{NH}_3)\text{MO}^{2+}$ and $(\text{NH}_3)_5\text{MO}^{2+}$ species ($M = \text{Ti-Cu}$), extending our previous work on the bare MO^{2+} ions. The potential energy curves along the M-O distance are constructed for the ground and multiple excited electronic states of $(\text{NH}_3)\text{MO}^{2+}$ and are compared to those of MO^{2+} . We see that ammonia stabilizes the oxo states ($\text{M}^{4+}\text{O}^{2-}$) over the oxyl ($\text{M}^{3+}\text{O}^{\cdot-}$) ones. This trend is intensified in the $(\text{NH}_3)_5\text{MO}^{2+}$ species. We then examined the reaction of the latter species with both methane and methanol. We find that the oxyl states activate a C-H bond easily with barriers smaller than 10 kcal/mol across all first-row transition metals, while the barriers for the oxo states start from about 50 kcal/mol for $M = \text{Ti}$ and decrease linearly to 10 kcal/mol going toward $M = \text{Ni}$. This is attributed to the increasing spin density on the oxygen atom observed for the oxo states. The most important finding is that the formation of hydrogen bonds between the OH group of methanol and the N-H bonds of the ammonia ligands increases the activation barriers for methanol considerably, making them comparable to and slightly higher than those of methane. This finding suggests a new strategy to slow the oxidation of methanol, leading to the long-desired higher methane-to-methanol selectivity.

KEYWORDS

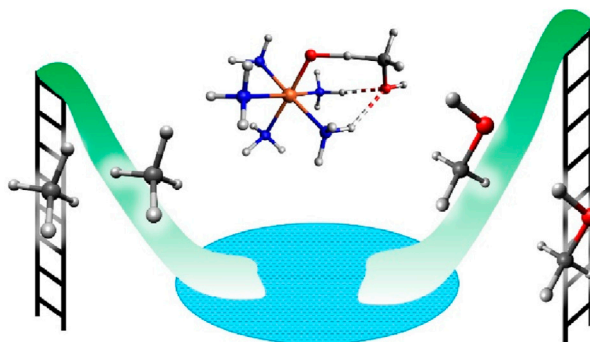
multireference approach, catalysis, methane-to-methanol, hydrogen bonding, ammonia ligand, first-row transition metal complexes

1 Introduction

Transition metal oxides have been widely studied in all forms, from bare diatomic species to molecular complexes and crystalline forms (heterogeneous catalysts). Bare (early) transition metal mono-oxides have been found in the observable regions of high-temperature outer planetary atmospheres and have been used to classify M supergiant (White and Wing, 1978; Merer, 1989; Sedaghati et al., 2017), while metal oxide molecular complexes and heterogeneous catalysts are promising candidates for a variety of industrial applications. The present computational work focuses on the role of molecular metal oxides in the purer conversion of methane to methanol, an important chemical transformation for cleaner energy solutions.

Earlier studies have investigated their electronic structure and reactivity with multireference, density functional theory (DFT), and machine learning methods (Periana et al., 1998; Gaggioli et al., 2019; Nandy et al., 2022). Molecular transition

TOC Graphic



GRAPHICAL ABSTRACT

metal oxides seem promising as potential catalysts for this process if certain issues can be overcome. One significant problem presented by Ravi et al. (2017) and Latimer et al. (2018) is that methanol continues to react, making formaldehyde and other overoxidized products. Therefore, both a method and a suitable catalyst need to be found to allow for efficient reactivity with a mechanism that prevents the oxidation of methanol. This presents a potential problem because the C-H bond of methanol is weaker than methane, so a proper catalyst and reaction are necessary to carry out the CH bond activation of methane without activating the methanol bonds (Gaggioli et al., 2019). No industrially viable solution has been identified to date, and only a few studies focus on the activation of methanol by metal oxides.

Transition metal oxide dications may be suitable catalysts for these processes due to their unique ability to switch between two forms: oxo ($M^{4+}O^{2-}$) and oxyl ($M^{3+}O^{\cdot-}$). (Claveau et al., 2023b). Nature chooses dications for several natural and biological processes, such as the heme iron complexes found in blood and in various enzymes (Hohenberger et al., 2012; Poulos, 2014; Ray et al., 2014; Martinie et al., 2017; Mitchell et al., 2017; Follmer et al., 2019). These dications have also important industrial applications (Hohenberger et al., 2012; Ray et al., 2014). The oxo form is characterized by a closed shell oxygen side, and the oxyl form has a significant electronic spin density on oxygen (Shimoyama and Kojima, 2019). Each form follows different reaction mechanisms. The oxo form will follow either the 2 + 2 mechanism or the proton-coupled electron transfer (PCET) mechanism. (Khan and Miliordos, 2021). Both of these mechanisms can be selective but usually possess high energy barriers that the reaction must overcome. The oxyl form utilizes the radical mechanism, otherwise known as hydrogen atom transfer (HAT) (Gaggioli et al., 2019). The HAT mechanism is not selective but is characterized by having low energy barriers.

Our group has done extensive analysis on transition metal oxide cations, neutral forms, and anions to understand their electronic structure and potential reactivity (Almeida et al., 2018; Ariyaratna and Miliordos, 2018; Claveau and Miliordos, 2019; Khan and Miliordos, 2019; Liu et al., 2019; Ariyaratna et al., 2020; Ariyaratna and Miliordos, 2020; Jackson and Miliordos, 2020;

Ariyaratna and Miliordos, 2021; Sader and Miliordos, 2021; Ariyaratna and Miliordos, 2022; Sader and Miliordos, 2022). Our computational work showed that anionic metal centers interact weakly with the produced methanol, which allows for its quick removal from the catalytic cycle to avoid overoxidation. Investigations into transition metal oxide dications have been ongoing for both first- and second-row transition metal oxides to categorize metals as oxo or oxyl based on their electronic structure as well as to explore their potential catalytic activity for methane activation (Kirkland et al., 2018; Almeida et al., 2019; Claveau and Miliordos, 2021; Khan and Miliordos, 2021; Claveau et al., 2023a).

The effect of different ligands on transition metal oxide dications to stabilize the oxo or oxyl character has begun to be investigated in the literature (Yang et al., 2014; Kirkland et al., 2018). A study of FeO^{2+} by Kirkland et al. (2018) showed that a strong field ligand, such as ammonia, can stabilize a higher energy oxo state to the ground state of the system (Kirkland et al., 2018). Yang et al. discuss a study of multiple $(H_2O)_6MO^{n+}$ complexes to resemble hematite, and of the dications mentioned (V-Cu), all had a higher spin ground state as a result of ligand attachment, indicating a possible correlation between ligand effects and metal oxide stabilization (Yang et al., 2014). It is expected that the 2 + 2 and PCET mechanisms will be favored with a strong field ligand such as ammonia, similar to what is shown in the FeO^{2+} study. On the other hand, the oxyl form and HAT mechanisms are preferred with electron-withdrawing ligands, such as halogens, as was demonstrated for ZrO (Jackson and Miliordos, 2020).

Many DFT studies have been done concerning the quantification of the oxophilicity, the ability to form a metal-oxygen bond, for transition metal oxides (Kepp, 2016; Moltved and Kepp, 2019; Deraet et al., 2021; Kayode and Montemore, 2021). Work has also been done at the DFT level using machine learning methods to try and characterize proper functionals to give a reliable description of the ground state for neutral transition metal oxides (Liu et al., 2020; Østrøm et al., 2022). Several multireference studies have been carried out on neutral and singly charged transition metal oxides; however, few studies exist for the dication systems, and they refer to bare (i.e., no ligand) systems

(Blomberg and Siegbahn, 1992; Nakao et al., 2001; Miliordos and Mavridis, 2010; Yang et al., 2014; Jiang et al., 2021).

Presently, our goal is to examine the electronic structure and reactivity of ligated MO^{2+} units, where M is a first-row transition metal. We are inspired by the work of Que and co-workers (Rasheed et al., 2018), who synthesized a series of FeO^{2+} complexes ($\text{N}_5\text{FeO}^{2+}$) with various ligands binding to the metal via tertiary (NR_3 , R = organic chain) or pyridinic nitrogen atoms (always forming a coordinative bond with their lone pair) and studied their reactivity toward methane activation. Similar complexes have been made for Ni, Mn, and Mo (Karunadasa et al., 2010; Leto et al., 2016; Bok et al., 2017). To simplify our calculations, we assess the replacement of the experimentally used ligands with simple ammonia for FeO^{2+} in terms of electronic structure and activation barriers for their reaction with methane, and we find minimal differences. We then study the reaction of these $(\text{NH}_3)_5\text{MO}^{2+}$ complexes with methanol (such studies are rare in the literature), and we find that the hydrogen bonding between the ammonia ligands and the incoming methanol (missing in the experimentally synthesized complexes) can make the difference. The complexes increase the activation barriers for methanol by ~ 20 kcal/mol or more and thus kinetically favor the activation of methane, suggesting higher overall selectivity for methanol production (smaller amounts of overoxidized products, such as formaldehyde), as happens for $(\text{NH}_3)_4\text{RhO}^{2+}$ (Claveau et al., 2023a). Ammonia ligands should be replaced by more applicable ligands for real-life applications, perhaps functionalizing existing ligands and adding OH or NH_2 groups, which will be the topic of future articles.

In Section 2, we discuss the computational approaches employed in this study. Section 3 discusses our results starting from mono-ligated $(\text{NH}_3)\text{MO}^{2+}$, which are compared with the bare MO^{2+} species we recently studied (Claveau and Miliordos, 2021). The interest then switches to the $(\text{NH}_3)_5\text{MO}^{2+}$ complexes, and the FeO^{2+} complexes are compared to the experimental $\text{N}_5\text{FeO}^{2+}$ species. Section 4 summarizes our conclusions.

2 Methods

We initially optimized the geometry of the ground state for each $(\text{NH}_3)\text{MO}^{2+}$ at the DFT/MN15 (Khan and Miliordos, 2019) level of theory with the cc-pVTZ (N,H,M)/aug-cc-pVTZ(O) (Dunning, 1989; Kendall et al., 1992; Woon and Dunning, 1994; Balabanov and Peterson, 2005) basis sets. The MN15 functional was used for this process, as it is designed for characterizing transition metals, and we have seen excellent consistency between MN15 and CCSD(T) results in the past regarding energetics for similar transition metal systems [see, for example, Claveau et al. (2023a) and Khan and Miliordos, 2019]. The aug-cc-pVTZ basis set is used on the oxygen to account for the polarized character of the metal–oxygen bond. Using this geometry, the potential energy curves as a function of the metal–oxygen distance are constructed via the complete active space self-consistent field (CASSCF) and multireference configuration interaction (MRCI) techniques. The active space of the reference CASSCF calculation consists of the three 2p orbitals of oxygen and the five 3d and one 4s orbitals of the metal, resulting in a nine-orbital active space. Electronic configurations were gathered at distances of interest

(minima, shoulders) for the ground and several low-lying excited states. All valence electrons were correlated with MRCI.

Calculations for the $(\text{NH}_3)_5\text{MO}^{2+}$ coordination complexes were carried out using Gaussian 16 software and the MN15 functional to first optimize the geometries, ensuring only real frequencies were returned from harmonic frequency calculations. The same triple- ζ basis was used here, and natural orbitals are analyzed at the same level of theory to describe the chemical bonding in the complexes. For the $\text{N}_5\text{FeO}^{2+}$ species, we used cc-pVDZ (N,H,M)/aug-cc-pVDZ(O) (Dunning, 1989; Kendall et al., 1992; Woon and Dunning, 1994; Balabanov and Peterson, 2005).

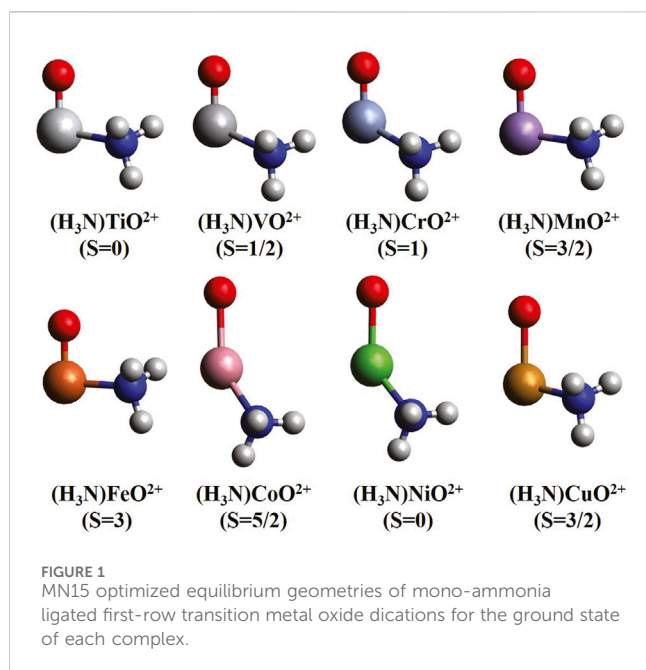
To investigate the reaction of these clusters with methane and methanol, the relative encounter complexes $[(\text{NH}_3)_5\text{MO}^{2+}(\text{CH}_4)]$ and transition states were also obtained for the lowest state of each spin multiplicity. The latter returned only one imaginary frequency from harmonic frequency calculations. These optimizations were completed using the same MN15/triple- ζ methodology.

All DFT and multireference calculations were completed using the Gaussian 16 and MOLPRO 2021 software packages, respectively (Werner et al., 2015; Frisch et al., 2016). All optimized geometries are given in Supplementary Tables S1–S9, S12, S13.

3 Results and discussion

3.1 $(\text{NH}_3)\text{MO}^{2+}$ species

Our earlier work on MO^{2+} revealed that the plain mono-oxides can be divided into three groups: early (M = Ti–Cr), middle (M = Mn, Fe), and late (M = Co–Cu) transition metals (Claveau and Miliordos, 2021). This separation is based on the electronic structure of the low-lying electronic states. The first group has well-defined $\text{M}^{4+}\text{O}^{2-}$ oxo ground states that are well separated from the $\text{M}^{3+}\text{O}^{\bullet-}$ oxyl excited states. Six of the valence electrons occupy the σ_{MO} and π_{MO} bonding orbitals ($\sigma_{\text{MO}}^2\pi_{\text{MO}}^4$), which are polarized toward oxygen, justifying an O^{2-} terminus. The remaining valence electrons populate the two δ_{M} orbitals, which are pure 3d orbitals of the metal ($\delta_{\text{M}}^{0,1,2}$ for Ti, V, and Cr, respectively), making the $X^1\Sigma^+$, $X^2\Delta$, and $X^3\Sigma^-/{}^1\Sigma^+/{}^1\Gamma$ electronic states of TiO^{2+} , VO^{2+} , and CrO^{2+} . The excited oxyl states are generated via a $\pi_{\text{MO}} \rightarrow \pi_{\text{MO}}^*$ (bonding \rightarrow antibonding) promotion, producing the ${}^1\Phi$, ${}^2\Pi$, and ${}^3\Sigma^-$ states of the three metal oxides. The π_{MO}^* orbitals have a dominant metallic 3d character. The emerged π_{MO}^1 electron creates the radical oxygen center. The middle metal oxides have ground states with long metal–oxygen bonds r_{MO} pointing to oxyl states ($r_{\text{MO}} > 2.0$ Å, ${}^{4,6,8}\Sigma^-$ states for MnO^{2+} and ${}^{3,5,7}\Delta$ for FeO^{2+}) but low-lying excited states of oxo character ($r_{\text{MO}} \sim 1.6$ Å, ${}^4\Pi$ for MnO^{2+} and ${}^5\Sigma^+$ for FeO^{2+}). In the oxo states, the additional electrons (compared to Cr) populate the π_{MO}^* instead of the half-filled δ_{M} orbitals. Finally, the late transition metal oxides have all long metal–oxygen bonds ($r_{\text{MO}} > 2.0$ Å) with no low-lying oxo states. It should be clarified that the π_{MO} orbitals change character, moving from Ti to Cu, shifting from highly localized on oxygen to highly localized on the metal, and the opposite happens for π_{MO}^* . This implies that the oxyl character should be assigned to a $(\pi_{\text{MO}}^*)^1$ configuration for the late transition metals (rather than π_{MO}^1). For the middle metals, both π_{MO} and π_{MO}^* have substantial contributions from both metallic and oxygen orbitals.



The optimized geometries for the $(\text{NH}_3)\text{MO}^{2+}$ ground states are shown in **Figure 1**. The ammonia ligand binds at an angle with respect to the MO bond, which varies from 93.9° ($M = \text{Fe}$) to 142° ($M = \text{Co}$). This NMO angle is not 180° as expected by conventional valence shell electron pair repulsion (VSEPR) arguments, even for $M = \text{Ti}$, which has no valence electrons on the metal. Although we cannot provide any explanation, it is related to the known trans-influence effect, according to which “ligands selectively weaken the bond trans to it” (Coe and Glenwright, 2000). The MO bond lengths are between 1.515 Å and 1.626 Å for Ti through Fe and between 2.001 Å and 2.079 Å for $M = \text{Co}$, Ni, and Cu. Compared to MO^{2+} , the bond lengths for early and late transition metals remain nearly unaffected when ammonia coordinates, unlike the middle metals where the bond distances contract from values larger than 2.0 Å to 1.626 Å ($M = \text{Mn}$) and 1.558 Å ($M = \text{Fe}$). This indicates that the oxo states are stabilized over the oxyl ones for these two metals, which is confirmed by our MRCI calculations and discussed further below. The C_s symmetry is imposed by rotating the ammonia ligand by no more than 20° for the subsequent CASSCF calculations.

The CASSCF active orbitals for the $(\text{NH}_3)\text{CrO}^{2+}$ and $(\text{NH}_3)\text{NiO}^{2+}$ species are shown in **Figure 2**. Due to the lower symmetry, the σ and one of the π orbitals of the MO bond belong to the same (a') irreducible representation, and in principle, they can be mixed, which is observed for the case of $\sigma_{\text{MO}}/\pi_{\text{MO}}$ or $1a'/2a'$ orbitals of $(\text{NH}_3)\text{CrO}^{2+}$ but not for $(\text{NH}_3)\text{NiO}^{2+}$. Generally, we were able to assign the a' and a'' orbitals as σ_{MO} , π_{MO} , σ_{MO}^* , π_{MO}^* , and δ_{M} . The $6a'$ orbital is minimally occupied in all cases and has a 3p character of oxygen (denoted as virt in **Figure 2**). This was included to account for the 4s orbital of the metal, which is not populated because the metal center is of either M^{4+} or M^{3+} nature.

The potential energy curves (PECs) for the MO stretching of the $(\text{NH}_3)\text{MO}^{2+}$ species have been constructed for several electronic states. The CASSCF PECs are shown in **Supplementary Figure S1** for all metals from Ti to Cu, and the MRCI PECs are given in **Figure 3**

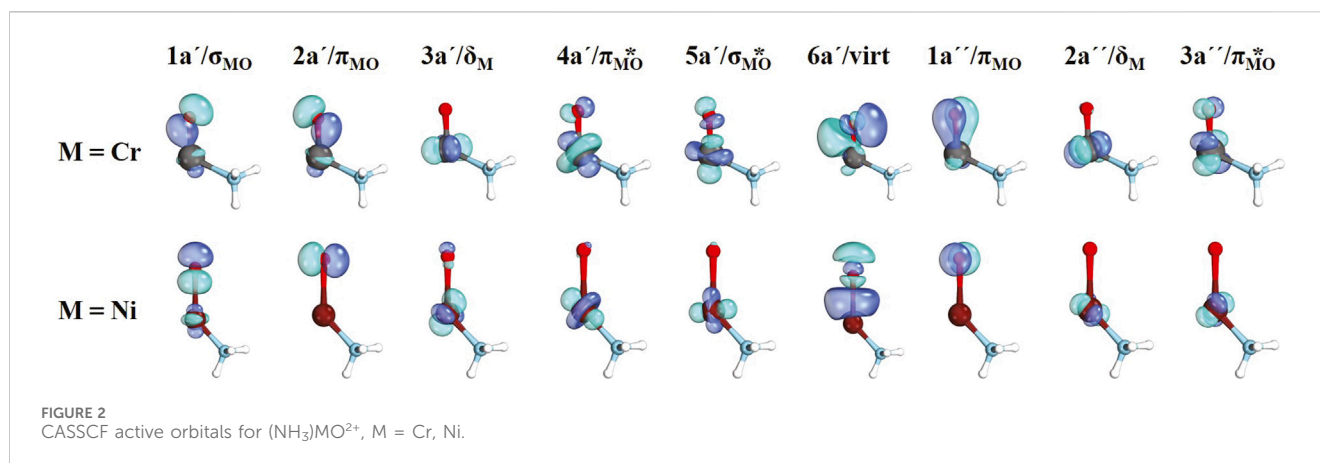
for Ti through Co. The PECs for the MO^{2+} diatomics are reported in **Claveau and Miliordos (2021)**. The addition of ammonia appears to have a smaller effect on the early transition metals (Ti–Cr). The morphology of the PECs remains the same before and after the inclusion of ammonia, with the difference being that the lower symmetry of $(\text{NH}_3)\text{MO}^{2+}$ leads to the splitting of the degenerate states of MO^{2+} . For example, the $^{1,3}\Pi$ and $^{1,3}\Phi$ ($\sigma_{\text{MO}}^2\pi_{\text{MO}}^3\pi_{\text{MO}}^{*1}$) excited states of TiO^{2+} split into the $^{1,3}A'$ and $^{1,3}A''$ components of $(\text{NH}_3)\text{TiO}^{2+}$, while the PEC of the ground state $^2\Delta$ for VO^{2+} separates into the lowest two $^2A'$ and $^2A''$ PECs of $(\text{NH}_3)\text{VO}^{2+}$. The splitting of the latter PECs is as large as 10 kcal/mol. On the other hand, the splitting for the $^1\Gamma$ excited state of CrO^{2+} is only 2 kcal/mol.

The position of the $M^{3+}\text{O}^{\bullet-}$ states relative to the ground $M^{4+}\text{O}^{2-}$ states shifts to higher energies. Specifically, the $^1\Sigma^+/^1A'$ ($M^{4+}\text{O}^{2-}$) \rightarrow $^1\Phi/^1A'$ ($M^{3+}\text{O}^{\bullet-}$) transitions for $\text{TiO}^{2+}/(\text{NH}_3)\text{TiO}^{2+}$ are approximately 50–60 kcal/mol. The same effect is observed for $\text{VO}^{2+}/(\text{NH}_3)\text{VO}^{2+}$ [$^2\Delta/^2(A', A'')$ vs. $^4\Delta/^4A''$]. For $(\text{NH}_3)\text{CrO}^{2+}$, the first excited oxo $^1\Gamma/^1(A', A'')$ states are clearly lower than the first oxyl $^3\Sigma^-/^3A''$ states in contrast with CrO^{2+} . This stabilization of oxo states over the oxyl states becomes more obvious for the middle transition metals ($M = \text{Mn}, \text{Fe}$). The $^4\Pi$ oxo state of MnO^{2+} is more than 20 kcal/mol higher than the clustered $^{4,6,8}\Sigma^-$ lowest oxyl states [see **Figure 1** of **Claveau and Miliordos (2021)**] but creates the local and global minima of the lowest energy $^4A''$ and $^4A'$ PECs, respectively, of $(\text{NH}_3)\text{MnO}^{2+}$ (see **Figure 3**). These are less than 13 kcal/mol higher than the global minimum of the oxyl character of the ground $^4A''$ state.

The case of iron is even more interesting because the $^5\Sigma^+$ oxo state of FeO^{2+} is 13 kcal/mol higher than the $^3\Delta$ ground oxyl state and becomes the ground $^5A'$ state of $(\text{NH}_3)\text{FeO}^{2+}$ separated by 4 kcal/mol from the first oxyl $^7A'$ state [pertaining to the $^7\Delta$ state of FeO^{2+} ; see **Figure 1** of **Claveau and Miliordos (2021)**]. This stabilization of the oxo state has been observed in the literature for the $(\text{NH}_3)\text{FeO}^{2+}/\text{FeO}^{2+}$ pair (Kirkland et al., 2018), but the present PECs are more complete, as they include more states, such as the aforementioned $^7A'$ state. In addition, comparing the CASSCF and MRCI PECs (**Figure 3; Supplementary Figure S1**) for iron, we see that the dynamic electron correlation is responsible for stabilizing the oxo states. Finally, in some of the PECs of $(\text{NH}_3)\text{CoO}^{2+}$ ($^4A'$ and $^4A''$), we see the appearance of local minima and shoulders at 1.6–1.7 Å and 20–23 kcal/mol, which are of oxo character. These were not present in CoO^{2+} and are expected to be stabilized even further when more ammonia ligands are coordinated to cobalt. The CASSCF/MRCI PECs for $(\text{NH}_3)\text{CoO}^{2+}$ show these shoulders at energies of approximately 40/20 kcal/mol above the global minimum. Such shoulders are not present at the CASSCF PECs for $(\text{NH}_3)\text{NiO}^{2+}$ and $(\text{NH}_3)\text{CuO}^{2+}$ (not at least within the 60 kcal/mol energy range of **Supplementary Figure S1**), and oxo minima are not expected to play an important role.

3.2 $(\text{NH}_3)_5\text{MO}^{2+}$ species

The addition of more ammonia ligands is expected to stabilize the electronic configurations corresponding to the oxo states. As a demonstration, we switch our discussion to the fully coordinated $(\text{NH}_3)_5\text{MO}^{2+}$ species. **Figure 4** depicts the frontier orbitals of



$(\text{NH}_3)_5\text{CrO}^{2+}$ and $(\text{NH}_3)_5\text{NiO}^{2+}$. We use the notation σ_{MO} , π_{MO} , σ_{MO}^* , π_{MO}^* , δ_{M} , and δ_{M}^* to facilitate the discussion and compare directly with the smaller metal oxide systems. The main difference going from MO^{2+} to $(\text{NH}_3)_5\text{MO}^{2+}$ is that one of the two non-bonding δ_{M} orbitals of MO^{2+} and $(\text{NH}_3)_5\text{MO}^{2+}$ becomes an antibonding metal–ammonia orbital (δ_{M}^*), and thus, the two δ_{M} orbitals are no longer degenerate, and the δ_{M}^* moves to higher energy between π_{MO}^* and σ_{MO}^* . The σ_{MO} and π_{MO} orbitals of $(\text{NH}_3)_5\text{MO}^{2+}$ are polarized toward oxygen, the δ_{M} and π_{MO}^* orbitals are equivalent to the t_{2g} orbitals for an O_h analog, and the δ_{M}^* and σ_{MO}^* correspond to the e_g orbitals. Note that the π_{MO} orbitals are polarized toward oxygen for both early and late transition metals, which is different from $\text{MO}^{2+}/(\text{NH}_3)_5\text{MO}^{2+}$; see, for example, $\pi_{\text{NiO}} \sim 3d_{\text{Ni}}$ [see Figure 2 of Claveau and Miliordos (2021)]. This is another indication that ammonia ligands stabilize the oxo character because the $\sigma_{\text{MO}}^2\pi_{\text{MO}}^4$ configuration can be assigned to $\text{M}^{4+}\text{O}^{2-}$ for both early and late transition metals. The π_{MO}^* orbitals have a higher contribution from the $3d$ orbitals of the metal for $(\text{NH}_3)_5\text{CrO}^{2+}$ as opposed to $(\text{NH}_3)_5\text{NiO}^{2+}$, which has a higher contribution from the $2p$ of oxygen. This is similar to the bare MO^{2+} species.

The metal–oxygen bond lengths (r_{MO}), relative energies, and electronic configurations for the lowest energy states of various spin multiplicities obtained with DFT are listed in Table 1. It should be noted that higher energy states for each spin multiplicity should generally exist in the energy range covered in Table 1 and are not currently included.

The electronic structure of $(\text{NH}_3)_5\text{TiO}^{2+}$ and $(\text{NH}_3)_5\text{VO}^{2+}$ closely resembles the structures of the plain or mono-ligated metal oxide dications. The ground states retain their $\sigma_{\text{MO}}^2\pi_{\text{MO}}^4$ and $\sigma_{\text{MO}}^2\pi_{\text{MO}}^4\delta_{\text{M}}^1$ oxo character being 50–60 kcal/mol away from the $\sigma_{\text{MO}}^2\pi_{\text{MO}}^3\delta_{\text{M}}^1$ and $\sigma_{\text{MO}}^2\pi_{\text{MO}}^3\delta_{\text{M}}^1\pi_{\text{MO}}^*$ oxyl states. The bond lengths reflect the bonding patterns: the oxo states have $r_{\text{MO}} = 1.579$ Å and 1.547 Å, whereas for the oxyl states, we obtained $r_{\text{MO}} = 1.841$ Å and 1.832 Å.

The electronic structure of the $(\text{NH}_3)_5\text{CrO}^{2+}$ lowest energy states is affected by the destabilization of δ_{M}^* . The ground state ($^3\Sigma^-$) of CrO^{2+} has a $\sigma_{\text{MO}}^2\pi_{\text{MO}}^4\delta_{\text{M}}^1\delta_{\text{M}}^*$ configuration (Claveau and Miliordos, 2021), but the lowest energy triplet of $(\text{NH}_3)_5\text{CrO}^{2+}$ adopts the $\sigma_{\text{MO}}^2\pi_{\text{MO}}^4\delta_{\text{M}}^1\pi_{\text{MO}}^*$ configuration, that is, δ_{M}^* is replaced by the lower energy π_{MO}^* orbital, which is still highly

localized on Cr (see Figure 4). However, the introduced antibonding orbital pushes the triplet state of $(\text{NH}_3)_5\text{CrO}^{2+}$ higher in energy than the singlet state ($\sigma_{\text{MO}}^2\pi_{\text{MO}}^4\delta_{\text{M}}^2$), which was an excited state for CrO^{2+} with more than 30 kcal/mol excitation energy. CrO^{2+} has two low-lying singlet states ($^1\Gamma$, $^1\Sigma^+$) made of all three $\sigma_{\text{MO}}^2\pi_{\text{MO}}^4(\delta_{\text{M}}\delta_{\text{M}}^*)^2$ singlet spin configurations (Claveau and Miliordos, 2021). Only the $\sigma_{\text{MO}}^2\pi_{\text{MO}}^4\delta_{\text{M}}^2$ configuration survives (no population of antibonding orbitals) for $(\text{NH}_3)_5\text{CrO}^{2+}$ and is the dominant configuration for the ground singlet state. The singlet and triplet states of $(\text{NH}_3)_5\text{CrO}^{2+}$ are within 1.8 kcal/mol and can be both categorized as oxo states with bond lengths of 1.520 ($S = 0$) Å and 1.613 ($S = 1$) Å. On the other hand, the quintet state of $(\text{NH}_3)_5\text{CrO}^{2+}$ has a bond length of 1.875 Å and a configuration $\sigma_{\text{MO}}^2\pi_{\text{MO}}^3\delta_{\text{M}}^1\pi_{\text{MO}}^*$, which makes it an oxyl state, and it is higher than the ground state by 20.2 kcal/mol.

The electronic structure changes dramatically for manganese as well. The $(\text{NH}_3)_5\text{MnO}^{2+}$ complex has oxo ground states as opposed to MnO^{2+} and $(\text{NH}_3)\text{MnO}^{2+}$, which have oxyl ground states and low-lying oxo states. The lowest doublet and quartet states of $(\text{NH}_3)_5\text{MnO}^{2+}$ have $\sigma_{\text{MO}}^2\pi_{\text{MO}}^3\delta_{\text{M}}^2\pi_{\text{MO}}^*$ and $\sigma_{\text{MO}}^2\pi_{\text{MO}}^4\delta_{\text{M}}^1\pi_{\text{MO}}^*$ configurations, respectively, with bond lengths 1.558 Å and 1.620 Å. The quartet state is the ground state separated by 4.2 kcal/mol from the doublet state. The sextet oxyl state is 13.6 kcal/mol higher with a bond length of 1.810 Å and a $\sigma_{\text{MO}}^2\pi_{\text{MO}}^3\delta_{\text{M}}^1\pi_{\text{MO}}^*\delta_{\text{M}}^*$ configuration. Overall, the oxo and oxyl states remain competitive, but the oxo states are more stable in the $(\text{NH}_3)_5\text{MnO}^{2+}$ complex.

The oxo states for iron are also stabilized further, going from $(\text{NH}_3)\text{FeO}^{2+}$ to $(\text{NH}_3)_5\text{FeO}^{2+}$. The $^5A'$ state of $(\text{NH}_3)_5\text{FeO}^{2+}$ with a $1a'^22a'^21a'^23a'^12a'^14a'^13a'^1$ (see Figure 2) $\sim \sigma_{\text{MO}}^2\pi_{\text{MO}}^4\delta_{\text{M}}^1\pi_{\text{MO}}^*\delta_{\text{M}}^*$ configuration (see Figure 4) remains among the lowest energy states, but two other states, a singlet and a triplet, where the two $3a'^13a'^1$ ($\sim \delta_{\text{M}}^1\delta_{\text{M}}^*$) electrons couple together in the δ_{M} orbital. The two π_{MO}^* electrons couple into an open-shell singlet or a triplet spin state. All three states are within 8 kcal/mol, and they have very similar r_{MO} values (1.60 ± 0.01 Å). The equatorial Fe–N bond lengths for the quintet state are longer, though (2.17 ± 0.02 Å vs. 2.03 Å), due to the population of the δ_{M}^* orbital, which has M–N antibonding character (see Figure 4). The open-shell singlet state has considerable spin contamination, and a more accurate description of the wave function necessitates applying multireference methods. The septet state is the lowest energy oxyl

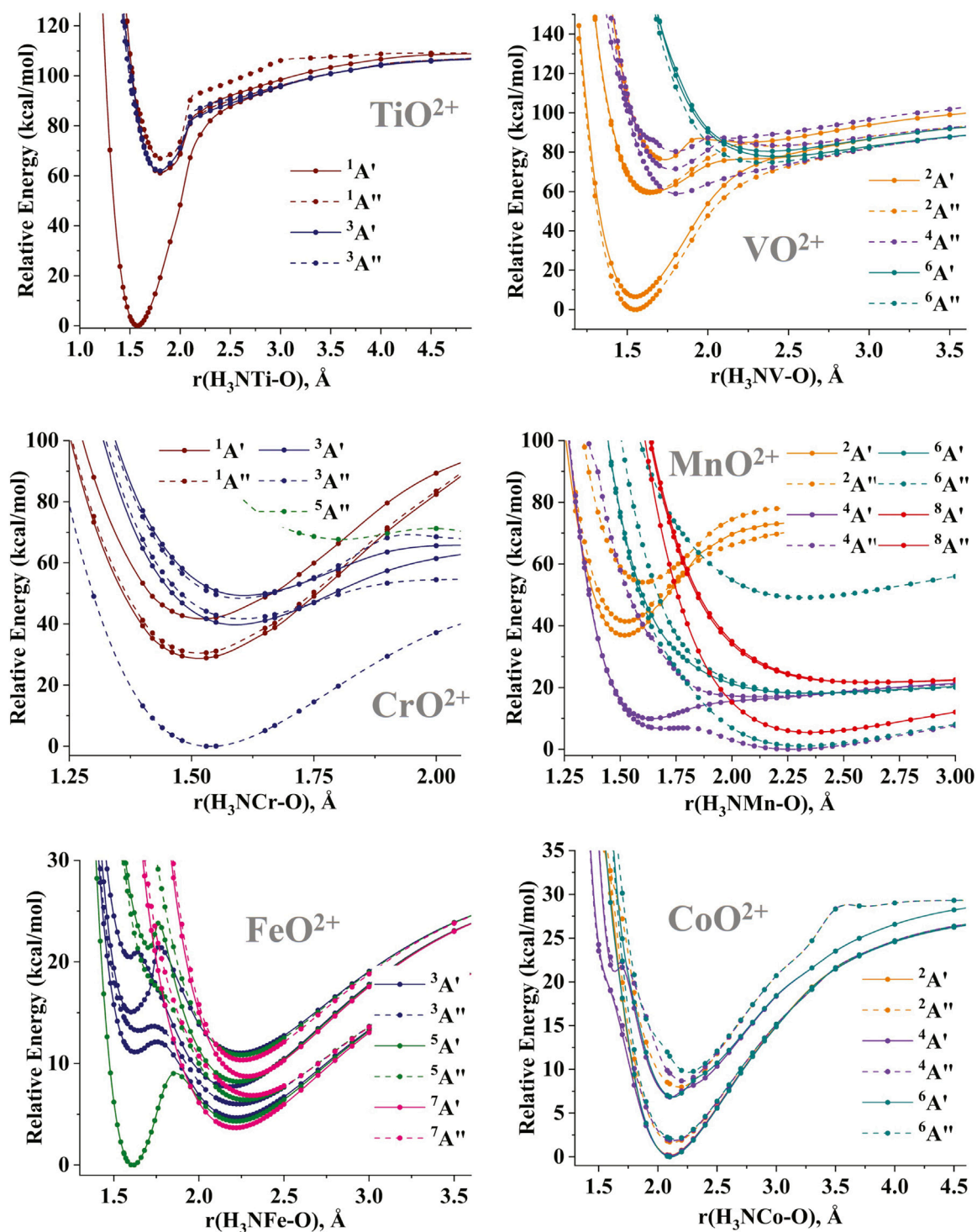
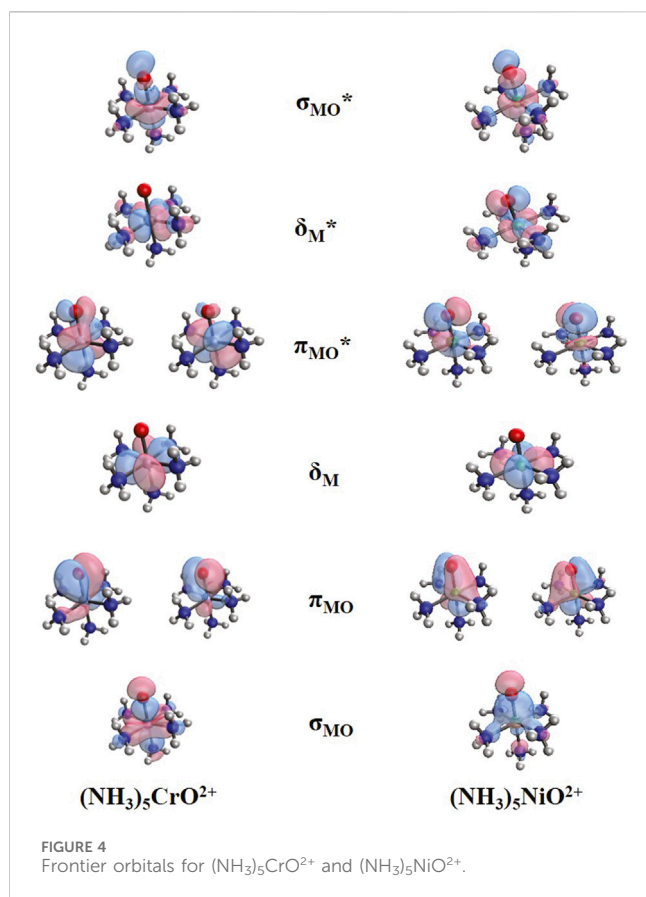


FIGURE 3
MRCI potential energy curves as a function of the M-O distance for the $(\text{NH}_3)_5\text{MO}^{2+}$ species, M = Ti-Co.

state, similar to $(\text{NH}_3)_5\text{FeO}^{2+}$, with a $\sigma_{\text{MO}}^2\pi_{\text{MO}}^3\delta_{\text{M}}^1\pi_{\text{MO}}^*{}^2\delta_{\text{M}}^*{}^1\sigma_{\text{MO}}^*{}^1$ configuration.

The lowest energy state of $(\text{NH}_3)_5\text{CoO}^{2+}$ is a doublet state with a bond length of 1.768 Å. This length lies in between the bond lengths encountered so far for oxo (~1.6 Å) and oxyl (>1.8 Å) states. Its configuration is $\sigma_{\text{MO}}^2\pi_{\text{MO}}^4\delta_{\text{M}}^2\pi_{\text{MO}}^*{}^3$, but now the π_{MO}^* orbital has a

larger contribution from the 2p of oxygen, similar to the $(\text{NH}_3)_5\text{NiO}^{2+}$ orbitals of Figure 4. Therefore, this is the first oxyl state not corresponding to a half-filled π_{MO} orbital; it has considerable Mulliken spin density on oxygen (1.0 electron). All the π_{MO}^3 states mentioned above have a spin density of 0.95 (except the S = 3 of iron, which has 1.45) on oxygen. In the quartet state, one



electron moves from π_{MO}^* to δ_{M}^* , which leads to the contraction of the MO bond to 1.643 Å and corresponds to the configuration of the shoulders observed in the PECs of $(\text{NH}_3)_5\text{CoO}^{2+}$ at around 20–25 kcal/mol (see above). Finally, the sextet state follows at 22.7 kcal/mol and populates σ_{MO}^* (spin density of 1.6).

Finally, all studied states of the last two oxides, $(\text{NH}_3)_5\text{NiO}^{2+}$ and $(\text{NH}_3)_5\text{CuO}^{2+}$, have long bond lengths (>1.75 Å), and their configurations have $\sigma_{\text{MO}}^2\pi_{\text{MO}}^4\delta_{\text{M}}^2$ in common. The remaining electrons populate the π_{MO}^* and δ_{M}^* orbitals, and the σ_{MO}^* is populated only for the highest spin states. The metal–oxygen bond in the quartet state of $(\text{NH}_3)_5\text{CuO}^{2+}$ is clearly ruptured and is better described as $(\text{NH}_3)_5\text{Cu}^{2+}+\text{O}$ (^3P). In all of these states, the spin density on oxygen is between 1.1 and 2.0; the spin density for $S = 3/2$ of $(\text{NH}_3)_5\text{CuO}^{2+}$ is 1.94.

3.3 $(\text{NH}_3)_5\text{MO}^{2+} + \text{CH}_4/\text{CH}_3\text{OH}$ reactions

Typical structures of the encounter complex of the reactants (R), the transition state (TS), and the encounter complex of the products (P) are shown in Figure 5. One H atom is transferred from CH_4 or CH_3OH radical is released as a product. Ideally, the reaction with methanol should be slower in order to avoid overoxidation of methanol and increase its yield. However, because the C–H bond of methane is stronger than that of methanol, the activation barrier for methanol is predisposed to be lower, posing significant difficulties in the search for selective catalysts. Recent experiments showed that establishing a

hydrophobic ligand environment can prevent methanol from approaching the metal center and increase the selectivity against formaldehyde (Fujisaki et al., 2023).

We suggested a different strategy in our recent computational work: The formation of hydrogen bonds between the OH group of methanol and the ligands can be exploited to increase the activation energy for methanol (Claveau et al., 2023a). Ammonia ligands can serve this role and are currently used as a model system. More applicable ligands, like the ones used to functionalize specific C–H bonds of complex organic by exploiting hydrogen bonding interactions (Olivo et al., 2017), will be explored in a future quest. Additionally, solvent effects are an important factor. For example, polar/non-polar solvents may disrupt/reinforce the hydrogen bonds between methanol and ligands.

As seen in Figure 5, in the case of $(\text{NH}_3)_5\text{MO}^{2+}$, the OH group of methanol makes two hydrogen bonds with two different ammonia ligands. To assess the importance of the formation of these hydrogen bonds, we considered some structures where the OH group points away from the ammonia ligands. All our efforts to obtain fully optimized structures with the OH away from ammonia ligands resulted in the formation of hydrogen bonds. Therefore, we started from the reactants and transition states of methane and replaced one H atom with an OH group, as shown in Figure 5C. The OH unit is optimized, but every other atom is kept fixed. These structures will be referred to as partially optimized (PO).

All our structures and energies are given in the SI. The resulting activation energies E_a , calculated as the energy difference between the TS and R energies, are plotted in Figure 6. These include all different spin states: low spin (LS; the lowest spin of Table 1), high spin (HS; the highest spin of Table 1; $S = 2$ for iron), and intermediate spin (IS; the spin between HS and LS of Table 1). The $S = 3$ state of $(\text{NH}_3)_5\text{FeO}^{2+}$ is also included. In all cases (except Ti/HS and Co/IS), E_a values are competitive (within 1.7 kcal/mol) for methane and methanol, and for these cases, the E_a value for methanol is larger. We could not get the TS for Ti/HS of methanol, and we are unsure why the E_a for methanol is lower than for methane by 6.4 kcal/mol in the case of Co/IS. These results indicate a different trend from the literature reports. For example, Nørskov and co-workers found that the E_a values for methanol are always 0.57 eV (13.1 kcal/mol) lower than methane for a large number/variety of heterogeneous catalysts. (Latimer et al., 2018). Similar differences can be implied for molecular catalysts based on the selectivity plots in Ravi et al. (2017). Our results confirm that hydrogen bonding can be a general future promising strategy that needs to be further explored (Claveau et al., 2023a).

The largest activation barriers for each metal correspond to states that have been characterized as oxo states, that is, LS of $(\text{NH}_3)_5\text{TiO}^{2+}$ and $(\text{NH}_3)_5\text{VO}^{2+}$, LS/IS for $(\text{NH}_3)_5\text{CrO}^{2+}$ and $(\text{NH}_3)_5\text{MnO}^{2+}$, and LS/IS/HS ($S = 2$) for $(\text{NH}_3)_5\text{FeO}^{2+}$. Interestingly, the E_a values for these states decrease in a linear fashion, going from early to late transition metals, which indicates that the radical character of the oxo states increases. This is also confirmed by the Mulliken spin densities on oxygen for these states: 0.00 (Ti/LS), 0.18 (V/LS), 0.00 (Cr/LS), 0.38 (Cr/IS), 0.06 (Mn/LS), 0.62 (Mn/IS), 0.00 (Fe/LS), 0.84 (Fe/IS), and 0.81 (Fe/HS). The Fe/LS state is the open-shell singlet sister state of Fe/IS, and thus, the spin density is 0.00 due to the cancelation of the two π_{MO}^* electron spins.

TABLE 1 Metal–oxygen bond length (r_{MO} in Å), relative energies (ΔE in kcal/mol), electronic configurations (see Figure 4 for orbitals), and Mulliken spin density on the oxygen atom (ρ_S/O) for the lowest energy spin states of $(NH_3)_5MO^{2+}$ species, M = Ti–Cu, at the MN15 level of theory.

Species	S	r_{MO}	ΔE	σ_{MO}	π_{MO}	π_{MO}^*	δ_M	π_{MO}^*	π_{MO}^*	δ_M^*	σ_{MO}^*	ρ_S/O
$(NH_3)_5TiO^{2+}$	0	1.579	0.0	2	2	2						0.00
	1	1.841	55.7	2	2	α	α					0.95
$(NH_3)_5VO^{2+}$	1/2	1.547	0.0	2	2	2	α					0.18
	3/2	1.832	54.2	2	2	α	α	α				0.96
$(NH_3)_5CrO^{2+}$	0	1.520	0.0	2	2	2	2					0.00
	1	1.613	1.8	2	2	2	α	α				0.38
	2	1.875	20.2	2	2	α	α	α	α			0.99
$(NH_3)_5MnO^{2+}$	1/2	1.558	4.2	2	2	2	2	α				0.06
	3/2	1.620	0.0	2	2	2	α	α	α			0.62
	5/2	1.810	13.6	2	2	α	α	α	α	α		0.96
$(NH_3)_5FeO^{2+}$	0 ^a	1.603	7.6	2	2	2	2	α	β			0.00
	1	1.602	0.0	2	2	2	2	α	α			0.84
	2	1.594	1.1	2	2	2	α	α	α	α		0.81
	3	1.878	23.3	2	2	α	α	α	α	α	α	1.45
$(NH_3)_5CoO^{2+}$	1/2	1.768	0.0	2	2	2	2	2	α			1.01
	3/2	1.643	4.5	2	2	2	2	α	α	α		1.18
	5/2	1.756	22.7	2	2	2	α	α	α	α	α	1.64
$(NH_3)_5NiO^{2+}$	0 ^a	1.759	1.0	2	2	2	2	2	α	β		1.14
	1	1.761	0.0	2	2	2	2	2	α	α		1.13
	2	1.777	9.2	2	2	2	2	α	α	α	α	1.77
$(NH_3)_5CuO^{2+}$	1/2	1.844	0.4	2	2	2	2	2	α	2		1.06
	3/2	2.546	0.0	2	2	2	2	2	α	α	α	1.94

^aThe spin contamination for these two open-shell singlets is 0.66 and 0.39 for $(NH_3)_5FeO^{2+}$ and $(NH_3)_5NiO^{2+}$, respectively.

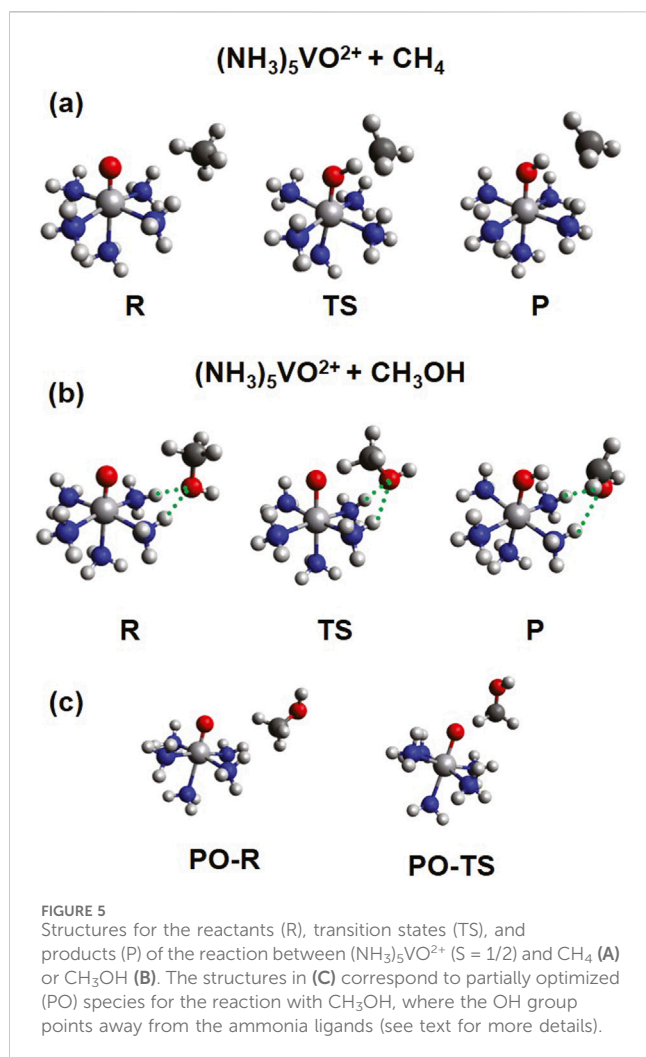
Notice that the 0.38 spin density of Cr/IS is responsible for lowering the barrier to less than half compared to the Cr/LS with 0.00 spin density. In contrast, although Mn/IS has a higher spin density on oxygen than Mn/LS (0.62 vs. 0.06), it has a higher activation barrier (25.6 vs. 15.5 kcal/mol). The reason is that the Mn/LS has a substantial contribution of a $\sigma_{MO}^2 \pi_{MO}^3 \delta_M^2 \pi_{MO}^*$ (in addition to the equilibrium $\sigma_{MO}^2 \pi_{MO}^4 \delta_M^2 \pi_{MO}^*$) electronic configuration at the transition state geometry. The partially occupied π_{MO} is the main reason for the lowering of the barrier, as happens for the Mn/HS ($\sigma_{MO}^2 \pi_{MO}^3 \delta_M^1 \pi_{MO}^* \delta_M^*$). This observation implies that a better quantity to consider is the spin density of the oxygen atom at the transition state of each species. These values are given in Supplementary Table S11. Indeed, the spin density for Mn/LS has dropped from 0.62 to 0.52, and that of Mn/IS has increased from 0.06 to 0.44. Plotting the average spin densities against the average E_a values over all oxo states for each species, we see a better correlation between E_a and transition state spin density on oxygen (see Supplementary Figure S4).

A different explanation can be provided based on the potential energy curves of Claveau et al. (2023b) along the reaction coordinate of $(NH_3)_5TiO^{2+} + CH_4$. According to Figure 7 and the

corresponding discussion of Claveau et al. (2023b), the activation barrier of the ground oxo state (Ti/LS/S = 0) is controlled by the excitation energy to the oxyl state (Ti/HS/S = 1). The lower the excitation energy, the lower the E_a value is expected to be. Indeed, the oxo \rightarrow oxyl energy difference drops as we go from Ti to Mn (55.7, 54.2, 20.2, and 13.6 kcal/mol; see Table 1) but increases for Fe (23.3 kcal/mol). Overall, the combination of the spin density on the oxygen atom (preferably at the transition states) and oxo \rightarrow oxyl excitation energies can be considered good descriptors for predicting the activation barriers of the reaction of metal oxides with methane.

On the other hand, the E_a values for the remaining states of clear oxyl character are very small (on the order of 10 kcal/mol or smaller) and present an increasing trend. The spin density on the oxygen atom is 0.95 or higher for these cases due to the partial occupation of the π_{MO} (for M = Ti–Fe) or π_{MO}^* (for M = Co, Ni) orbitals (see Table 1), which are primarily composed of the 2p orbitals of oxygen (see Figure 4). The two lines (oxo and oxyl) converge to the same values for $(NH_3)_5NiO^{2+}$ (see Figure 6).

The reason for the unprecedentedly high activation barriers for methanol has been ascribed to the disruption of both the hydrogen bonds and the “stress” imposed on the activated CH bond going



from the reactants to the TS, as expressed by the increased hydrogen bond distances and the decreased OCH angles (Claveau et al., 2023a). The same observations can be made here. The latter angles range between 176° and 180° for CH₄ (no hydrogen bonding) and between 166° and 175° for CH₃OH (see Supplementary Figure S2). Finally, we compare the activation barriers for methanol using the fully and partially optimized structures for R and TS (see Figure 5). In several cases, the E_a values for the partially optimized structures are negative because these structures do not correspond to actual stationary structures. The E_a values for the two cases and their differences are plotted in Supplementary Figure S3. The difference between the two structures is remarkably consistent across the various metals and spin states ranging between 17 kcal/mol and 22 kcal/mol. This is a very large difference that can play an important role in developing strategies for the selective formation of methanol.

3.4 (NH₃)₅FeO²⁺ vs. N₅FeO²⁺

In this section, we compare the all-ammonia iron oxide complex with the experimental structures of Rasheed et al. (2018), which bear

tertiary and pyridinic N-ligands (see Figure 7). This comparison serves two purposes. First, we assess the use of ammonia as a simple model ligand to replace tertiary and pyridinic N-ligands, and second, we calculate the activation barriers for methane and methanol in a ligand environment (N₅FeO²⁺) where hydrogen bond formation is not possible.

The lowest energy state of N₅FeO²⁺ is the triplet, followed closely by the quintet (at 6.2 kcal/mol) and singlet (at 7.2 kcal/mol) states. The septet is well separated at 32.0 kcal/mol. This pattern is identical to (NH₃)₅FeO²⁺, and the numerical values agree well for the two species: 1.1 kcal/mol vs. 6.2 kcal/mol, 7.6 kcal/mol vs. 7.2 kcal/mol, and 23.3 kcal/mol vs. 32.0 kcal/mol (see Table 1). Overall, the electronic effects associated with the pyridinic rings (possible π -back bonding) have some effect on the electronic structure of the iron oxide unit, but ammonia can clearly provide big-picture insights at a significantly lower computational cost. Of course, ammonia ligands cannot account for steric effects or other types of interactions (such as dispersion) present in larger ligands (see next paragraph). In summary, we believe that the relative energetics provided in Table 1 for the various spin states of (NH₃)₅MO²⁺ are valid for the N₅MO²⁺ species as well.

The transition states for the reaction of N₅FeO²⁺ with methane and methanol are depicted in Figure 7. The two molecules approach N₅FeO²⁺ with the same orientation because the OH group of methanol interacts only weakly with the pyridinic rings. The OH/CH distances at the transition states are 1.20/1.33 Å and 1.28/1.28 Å for methane and methanol, respectively, indicating that the H atom departs “earlier” from methanol. The activation barriers for methane are 24.6 kcal/mol and 24.5 kcal/mol for the triplet and quintet states, which are higher by 3.7 kcal/mol and 5.5 kcal/mol than (NH₃)₅FeO²⁺ (see Supplementary Table S10), possibly because of the dispersion interactions between CH₄ and the π -system of the pyridinic rings. The activation barriers for methanol of 22.5 kcal/mol (for both spin multiplicities) are lower than methane, signifying again the importance of hydrogen bonding in the (NH₃)₅FeO²⁺ species.

4 Conclusion

In this work, we studied the electronic structure and reactivity of the dicationic transition metal oxide complexes (NH₃)₅MO²⁺, where M is a first-row transition metal. We started by extending our previous work on the bare metal oxide unit, MO²⁺, to the mono-ligated (NH₃)MO²⁺ species. In both cases, we have constructed potential energy curves along the M-O distance for the ground and numerous excited electronic states. We covered a sufficiently wide energy range to include both oxo (M⁴⁺O²⁻) and oxyl (M³⁺O⁻) electronic states. We concluded that the ammonia ligand stabilizes the oxo states. For the early transition metals (Ti, V, and Cr), the oxo states, already lower in energy for MO²⁺, become more well separated from the oxyl states. For the middle transition metals (Mn, Fe), the oxo states (higher in energy for MO²⁺) become energetically competitive with the oxyl states (Mn) or the ground state (Fe). The lowest states for the late transition metals remain of oxyl character, but for Co, we see some shoulders in the repulsive region of the potential energy curves corresponding to oxo electronic configurations. The dynamic electron correlation (at

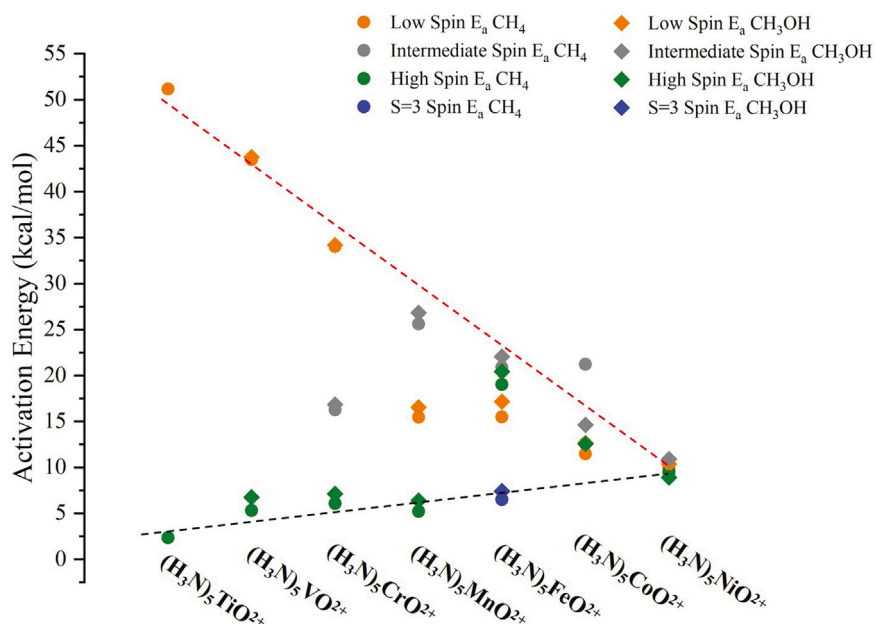


FIGURE 6
 Activation energies (E_a) for the reactions of $(\text{NH}_3)_5\text{MO}^{2+}$ with CH_4 and CH_3OH for $M = \text{Ti-Ni}$ and for LS, IS, and HS spin states, and $S = 3$ of $M = \text{Fe}$. The dashed red/black lines show the trend for oxo/oxyl states. All numerical values are listed in [Supplementary Table S10](#) of the SI.

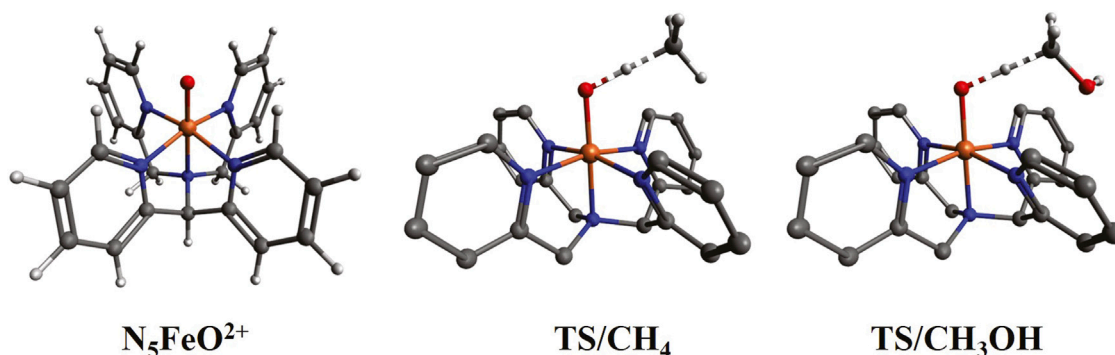


FIGURE 7
 Optimized structures for $\text{N}_5\text{FeO}^{2+}$ (triplet ground state) and the transition states (TS) of its reaction with CH_4 and CH_3OH . The hydrogen atoms of $\text{N}_5\text{FeO}^{2+}$ are not shown in the TS structures.

the MRCI level) was found to be important for the stabilization of the oxo states.

We then switched to the fully coordinated $(\text{NH}_3)_5\text{MO}^{2+}$ complexes, where we applied DFT to study the lowest energy state of low-, intermediate-, and high-spin multiplicity. The coordination of more ammonia ligands stabilized the oxo states even further. For both early and middle transition metals, the ground states are of oxo character (low and intermediate spin), followed by the high-spin oxyl states at energies ~ 55 kcal/mol for Ti and V and 14–23 kcal/mol for Cr, Mn, and Fe. The coordination of five ammonia ligands to CoO^{2+} stabilized the states observed as shoulders in $(\text{NH}_3)\text{CoO}^{2+}$, creating a clear minimum (intermediate spin). Going from MO^{2+} to $(\text{NH}_3)\text{MO}^{2+}$, we see that the π_{MO}^* and one δ_{M} orbitals become the pseudo- t_{2g} orbitals, and the σ_{MO}^* and the other δ_{M} (δ_{M}^*) become the pseudo- e_g ones. Therefore, the low-lying electronic states of $(\text{NH}_3)_5\text{MO}^{2+}$ can be generally predicted from

these of MO^{2+} , considering that the energy of the MO^{2+} states that populate the δ_{M}^* increases appreciably.

We then probed the reactivity of all studied $(\text{NH}_3)_5\text{MO}^{2+}$ electronic states regarding the activation of methane and methanol. We found the activation barriers for the oxo states are considerably higher for the early transition metals. The barriers for the oxo states drop as we move to the later transition metals. The barriers for the oxyl states are small (< 10 kcal/mol) and show a slightly increasing trend as we move from the early to the late transition metals. Based on the spin density on the oxygen atom, we ascribed these trends to the fact that the oxyl character of the oxo states increases as we move to the later metals. Therefore, the two sets of barriers converge almost linearly, going from Ti to Ni.

The reaction with methanol, rarely studied in the literature, is important for identifying catalysts for the selective transformation of

methane to methanol. Catalysts with higher activation barriers for methanol will slow its overoxidation and avoid the formation of formaldehyde. Here, we show that the hydrogen bonds between the OH group of methanol and the ammonia ligands may increase the barrier for methanol by about 20 kcal/mol, rendering it slightly higher than (or at least competitive with) that of methane.

Finally, we performed calculations for the experimentally made N_5FeO^{2+} complex, where five ligands (four pyridinic rings and one tertiary nitrogen) make coordinative bonds with iron via a nitrogen center, but they cannot form hydrogen bonds with methanol. We showed that the electronic structure and energetics of the lowest lying states of $(NH_3)_5FeO^{2+}$ and N_5FeO^{2+} follow the same pattern and that methanol goes through a higher activation barrier for the former and lower for the latter compared to methane.

Our future work will focus on more applicable ligands to assess the effect of all kinds of interactions (hydrogen bonding, dispersion, electrostatic, and others) in the activation barriers of methane and methanol to identify systems with much larger barriers for methanol. The role of solvent molecules will also be explored. We believe that our findings provide an additional arrow to the chemists' quiver and will lead to the design of more practical ligands with even higher activation barriers for methanol.

Data availability statement

The original contributions presented in the study are included in the article/[Supplementary Material](#); further inquiries can be directed to the corresponding author.

Author contributions

EC: data curation, formal analysis, investigation, visualization, and writing—review and editing. EM: conceptualization, formal analysis, supervision, writing—original draft, and writing—review and editing.

References

- Almeida, N. M. S., Ariyaratna, I. R., and Miliordos, E. (2018). *Ab initio* calculations on the ground and excited electronic states of neutral and charged palladium monoxide, $PdO_{0,+,-}$. *Phys. Chem. Chem. Phys.* 20, 14578–14586. doi:10.1039/c8cp01251b
- Almeida, N. M. S., Ariyaratna, I. R., and Miliordos, E. (2019). O–H and C–H bond activations of water and methane by RuO_2^+ and $(NH_3)RuO_2^+$: ground and excited states. *J. Phys. Chem. A* 123, 9336–9344. doi:10.1021/acs.jpca.9b05910
- Ariyaratna, I. R., Almeida, N. M. S., and Miliordos, E. (2020). *Ab initio* investigation of the ground and excited states of RuO_2^+ and their reaction with water. *Phys. Chem. Chem. Phys.* 22, 16072–16079. doi:10.1039/d0cp02468f
- Ariyaratna, I. R., and Miliordos, E. (2018). *Ab initio* investigation of the ground and excited states of $MoO_4^{2+,-}$ and their catalytic strength on water activation. *Phys. Chem. Chem. Phys.* 20, 12278–12287. doi:10.1039/c8cp01676c
- Ariyaratna, I. R., and Miliordos, E. (2020). *Ab initio* investigation of the ground and excited states of ZrO_4^+ and NbO_4^+ . *J. Quantitative Spectrosc. Radiat. Transf.* 255, 107265. doi:10.1016/j.jqsrt.2020.107265
- Ariyaratna, I. R., and Miliordos, E. (2021). Radical abstraction vs. oxidative addition mechanisms for the activation of the S–H, O–H, and C–H bonds using early transition metal oxides. *Phys. Chem. Chem. Phys.* 23, 1437–1442. doi:10.1039/d0cp05513a
- Ariyaratna, I. R., and Miliordos, E. (2022). *Ab initio* investigation of the ground and excited states of TcO_4^+ and RhO_4^+ . *J. Quantitative Spectrosc. Radiat. Transf.* 280, 108074. doi:10.1016/j.jqsrt.2022.108074
- Balabanov, N. B., and Peterson, K. A. (2005). Systematically convergent basis sets for transition metals. I. All-electron correlation consistent basis sets for the 3d elements Sc–Zn. *J. Chem. Phys.* 123, 064107. doi:10.1063/1.1998907
- Blomberg, M. R. A., and Siegbahn, P. E. M. (1992). A comparison between multireference CI and effective medium theories for diatomic FeN. *Theor. Chim. Acta* 81, 365–374. doi:10.1007/bf01134861
- Bok, K. H., Lee, M. M., You, G. R., Ahn, H. M., Ryu, K. Y., Kim, S.-J., et al. (2017). Synthesis, characterization, and catalytic activities of a nickel(II) monoamido-tetradentate complex: evidence for Ni(III)-oxo and Ni(IV)-oxo species. *Chem. – A Eur. J.* 23, 3117–3125. doi:10.1002/chem.201605157
- Claveau, E. E., Heller, E. R., Richardson, J. O., and Miliordos, E. (2023a). Methane against methanol: the tortoise and the hare of the oxidation race. *J. Phys. Chem. Lett.* 14, 8749–8754. doi:10.1021/acs.jpcclett.3c02274
- Claveau, E. E., and Miliordos, E. (2019). Quantum chemical calculations on NbO and its reaction with methane: ground and excited electronic states. *Phys. Chem. Chem. Phys.* 21, 26324–26332. doi:10.1039/c9cp05408a
- Claveau, E. E., and Miliordos, E. (2021). Electronic structure of the dicationic first row transition metal oxides. *Phys. Chem. Chem. Phys.* 23, 21172–21182. doi:10.1039/d1cp02492b
- Claveau, E. E., Sader, S., Jackson, B. A., Khan, S. N., and Miliordos, E. (2023b). Transition metal oxide complexes as molecular catalysts for selective methane to

Funding

The author(s) declare that financial support was received for the research, authorship, and/or publication of this article. The authors are indebted to Auburn University (AU) for financial support. EM is especially grateful to the donors of the James E. Land endowment. This work was completed using resources provided by the Auburn University Hopper and Easley Clusters.

Conflict of interest

The authors declare that the research was conducted in the absence of any commercial or financial relationships that could be construed as a potential conflict of interest.

Generative AI statement

The author(s) declare that no generative AI was used in the creation of this manuscript.

Publisher's note

All claims expressed in this article are solely those of the authors and do not necessarily represent those of their affiliated organizations, or those of the publisher, the editors, and the reviewers. Any product that may be evaluated in this article, or claim that may be made by its manufacturer, is not guaranteed or endorsed by the publisher.

Supplementary material

The Supplementary Material for this article can be found online at: <https://www.frontiersin.org/articles/10.3389/fchem.2024.1508515/full#supplementary-material>

- methanol transformation: any prospects or time to retire? *Phys. Chem. Chem. Phys.* 25, 5313–5326. doi:10.1039/d2cp05480a
- Coe, B. J., and Glenwright, S. J. (2000). Trans-effects in octahedral transition metal complexes. *Coord. Chem. Rev.* 203, 5–80. doi:10.1016/s0010-8545(99)00184-8
- Deraet, X., Turek, J., Alonso, M., Tielens, F., Cottenier, S., Ayers, P. W., et al. (2021). Reactivity of single transition metal atoms on a hydroxylated amorphous silica surface: a periodic conceptual DFT investigation. *Chem. – A Eur. J.* 27, 6050–6063. doi:10.1002/chem.202004660
- Dunning, T. H., Jr. (1989). Gaussian basis sets for use in correlated molecular calculations. I. The atoms boron through neon and hydrogen. *J. Chem. Phys.* 90, 1007–1023. doi:10.1063/1.456153
- Follmer, A. H., Tripathi, S., and Poulos, T. L. (2019). Ligand and redox partner binding generates a new conformational state in cytochrome P450cam (CYP101A1). *J. Am. Chem. Soc.* 141, 2678–2683. doi:10.1021/jacs.8b13079
- Frisch, M. J., Trucks, G. W., Schlegel, H. B., Scuseria, G. E., Robb, M. A., Cheeseman, J. R., et al. (2016). *Gaussian 16 rev. B.01*. Wallingford, CT.
- Fujisaki, H., Ishizuka, T., Kotani, H., Shiota, Y., Yoshizawa, K., and Kojima, T. (2023). Selective methane oxidation by molecular iron catalysts in aqueous medium. *Nature* 616, 476–481. doi:10.1038/s41586-023-05821-2
- Gaggioli, C. A., Sauer, J., and Gagliardi, L. (2019). Hydrogen atom or proton coupled electron transfer? C–H bond activation by transition-metal oxides. *J. Am. Chem. Soc.* 141, 14603–14611. doi:10.1021/jacs.9b04006
- Hohenberger, J., Ray, K., and Meyer, K. (2012). The biology and chemistry of high-valent iron–oxo and iron–nitrido complexes. *Nat. Commun.* 3, 720. doi:10.1038/ncomms1718
- Jackson, B. A., and Miliordos, E. (2020). Weak-field ligands enable inert early transition metal oxides to convert methane to methanol: the case of ZrO. *Phys. Chem. Chem. Phys.* 22, 6606–6618. doi:10.1039/c9cp06050b
- Jiang, T., Chen, Y., Bogdanov, N. A., Wang, E., Alavi, A., and Chen, J. (2021). A full configuration interaction quantum Monte Carlo study of ScO, TiO, and VO molecules. *J. Chem. Phys.* 154, 164302. doi:10.1063/5.0046464
- Karunadasa, H. I., Chang, C. J., and Long, J. R. (2010). A molecular molybdenum-oxo catalyst for generating hydrogen from water. *Nature* 464, 1329–1333. doi:10.1038/nature08969
- Kayode, G. O., and Montemore, M. M. (2021). Factors controlling oxophilicity and carbophilicity of transition metals and main group metals. *J. Mater. Chem. A* 9, 22325–22333. doi:10.1039/d1ta06453c
- Kendall, R. A., Dunning, T. H., Jr., and Harrison, R. J. (1992). Electron affinities of the first-row atoms revisited. Systematic basis sets and wave functions. *J. Chem. Phys.* 96, 6796–6806. doi:10.1063/1.462569
- Kepp, K. P. (2016). A quantitative scale of oxophilicity and thiophilicity. *Inorg. Chem.* 55, 9461–9470. doi:10.1021/acs.inorgchem.6b01702
- Khan, S. N., and Miliordos, E. (2019). Methane to methanol conversion facilitated by transition-metal methyl and methoxy units: the cases of FeCH₃⁺ and FeOCH₃⁺. *J. Phys. Chem. A* 123, 5590–5599. doi:10.1021/acs.jpca.9b04005
- Khan, S. N., and Miliordos, E. (2021). Electronic structure of RhO₂⁺, its ammoniated complexes (NH₃)_{1–5}RhO₂⁺, and mechanistic exploration of CH₄ activation by them. *Inorg. Chem.* 60, 16111–16119. doi:10.1021/acs.inorgchem.1c01447
- Kirkland, J. K., Khan, S. N., Casale, B., Miliordos, E., and Vogiatzis, K. D. (2018). Ligand field effects on the ground and excited states of reactive FeO₂⁺ species. *Phys. Chem. Chem. Phys.* 20, 28786–28795. doi:10.1039/c8cp05372c
- Latimer, A. A., Kakekhani, A., Kulkarni, A. R., and Nørskov, J. K. (2018). Direct methane to methanol: the selectivity–conversion limit and design strategies. *ACS Catal.* 8, 6894–6907. doi:10.1021/acscatal.8b00220
- Leto, D. F., Massie, A. A., Rice, D. B., and Jackson, T. A. (2016). Spectroscopic and computational investigations of a mononuclear manganese(IV)-Oxo complex reveal electronic structure contributions to reactivity. *J. Am. Chem. Soc.* 138, 15413–15424. doi:10.1021/jacs.6b08661
- Liu, F., Duan, C., and Kulik, H. J. (2020). Rapid detection of strong correlation with machine learning for transition-metal complex high-throughput screening. *J. Phys. Chem. Lett.* 11, 8067–8076. doi:10.1021/acs.jpcclett.0c02288
- Liu, G., Zhu, Z., Ciborowski, S. M., Ariyaratna, I. R., Miliordos, E., and Bowen, K. H. (2019). Selective activation of the C–H bond in methane by single platinum atomic anions. *Angew. Chem. Int. Ed.* 58, 7773–7777. doi:10.1002/anie.201903252
- Martinie, R. J., Pollock, C. J., Matthews, M. L., Bollinger, J. M., Jr., Krebs, C., and Silakov, A. (2017). Vanadyl as a stable structural mimic of reactive ferryl intermediates in mononuclear nonheme-iron enzymes. *Inorg. Chem.* 56, 13382–13389. doi:10.1021/acs.inorgchem.7b02113
- Merer, A. J. (1989). Spectroscopy of the diatomic 3d transition metal oxides. *Annu. Rev. Phys. Chem.* 40, 407–438. doi:10.1146/annurev.physchem.40.1.407
- Miliordos, E., and Mavridis, A. (2010). Electronic structure and bonding of the early 3d-transition metal diatomic oxides and their ions: ScO_{0,±}, TiO_{0,±}, CrO_{0,±}, and MnO_{0,±}. *J. Phys. Chem. A* 114, 8536–8572. doi:10.1021/jp910218u
- Mitchell, A. J., Dunham, N. P., Martinie, R. J., Bergman, J. A., Pollock, C. J., Hu, K., et al. (2017). Visualizing the reaction cycle in an iron(II)- and 2-(Oxo)-glutarate-Dependent hydroxylase. *J. Am. Chem. Soc.* 139, 13830–13836. doi:10.1021/jacs.7b07374
- Moltved, K. A., and Kepp, K. P. (2019). The chemical bond between transition metals and oxygen: electronegativity, d-orbital effects, and oxophilicity as descriptors of metal–oxygen interactions. *J. Phys. Chem. C* 123, 18432–18444. doi:10.1021/acs.jpcc.9b04317
- Nakao, Y., Hirao, K., and Taketsugu, T. (2001). Theoretical study of first-row transition metal oxide cations. *J. Chem. Phys.* 114, 7935–7940. doi:10.1063/1.1362323
- Nandy, A., Duan, C., Goffinet, C., and Kulik, H. J. (2022). New strategies for direct methane-to-methanol conversion from active learning exploration of 16 million catalysts. *JACS Au* 2, 1200–1213. doi:10.1021/jacsau.2c00176
- Olivo, G., Farinelli, G., Barbieri, A., Lanzalunga, O., Di Stefano, S., and Costas, M. (2017). Supramolecular recognition allows remote, site-selective C–H oxidation of methylenic sites in linear amines. *Angew. Chem. Int. Ed.* 56, 16347–16351. doi:10.1002/anie.201709280
- Østrøm, I., Hossain, M. A., Burr, P. A., Hart, J. N., and Hoex, B. (2022). Designing 3d metal oxides: selecting optimal density functionals for strongly correlated materials. *Phys. Chem. Chem. Phys.* 24, 14119–14139. doi:10.1039/d2cp01303g
- Periana, R. A., Taube, D. J., Gamble, S., Taube, H., Satoh, T., and Fujii, H. (1998). Platinum catalysts for the high-yield oxidation of methane to a methanol derivative. *Science* 280, 560–564. doi:10.1126/science.280.5363.560
- Poulos, T. L. (2014). Heme enzyme structure and function. *Chem. Rev.* 114, 3919–3962. doi:10.1021/cr400415k
- Rasheed, W., Draksharapu, A., Banerjee, S., Young Jr, V. G., Fan, R., Guo, Y., et al. (2018). Crystallographic evidence for a sterically induced ferryl tilt in a non-heme oxoiron(IV) complex that makes it a better oxidant. *Angew. Chem. Int. Ed.* 57, 9387–9391. doi:10.1002/anie.201804836
- Ravi, M., Ranocchiaro, M., and Van Bokhoven, J. A. (2017). The direct catalytic oxidation of methane to methanol—a critical assessment. *Angew. Chem. Int. Ed.* 56, 16464–16483. doi:10.1002/anie.201702550
- Ray, K., Pfaff, F. F., Wang, B., and Nam, W. (2014). Status of reactive non-heme metal–oxygen intermediates in chemical and enzymatic reactions. *J. Am. Chem. Soc.* 136, 13942–13958. doi:10.1021/ja507807v
- Sader, S., and Miliordos, E. (2021). Methane to methanol conversion facilitated by anionic transition metal centers: the case of Fe, Ni, Pd, and Pt. *J. Phys. Chem. A* 125, 2364–2373. doi:10.1021/acs.jpca.0c10577
- Sader, S., and Miliordos, E. (2022). Being negative can be positive: metal oxide anions promise more selective methane to methanol conversion. *Phys. Chem. Chem. Phys.* 24, 21583–21587. doi:10.1039/d2cp02771b
- Sedaghati, E., Boffin, H. M. J., Macdonald, R. J., Gandhi, S., Madhusudhan, N., Gibson, N. P., et al. (2017). Detection of titanium oxide in the atmosphere of a hot Jupiter. *Nature* 549, 238–241. doi:10.1038/nature23651
- Shimoyama, Y., and Kojima, T. (2019). Metal–oxyl species and their possible roles in chemical oxidations. *Inorg. Chem.* 58, 9517–9542. doi:10.1021/acs.inorgchem.8b03459
- Werner, H.-J., Knowles, P. J., Knizia, G., Manby, F. R., Schütz, M., Celani, P., et al. (2015). MOLPRO, version 2015.1, a package of *ab initio* programs.
- White, N. M., and Wing, R. F. (1978). Photoelectric two-dimensional spectral classification of M supergiants. *Astrophysical J.* 222, 209–219. doi:10.1086/156136
- Woon, D. E., and Dunning, T. H., Jr. (1994). Gaussian basis sets for use in correlated molecular calculations. IV. Calculation of static electrical response properties. *J. Chem. Phys.* 100, 2975–2988. doi:10.1063/1.466439
- Yang, Y., Ratner, M. A., and Schatz, G. C. (2014). Multireference *ab initio* study of ligand field d–d transitions in octahedral transition-metal oxide clusters. *J. Phys. Chem. C* 118, 29196–29208. doi:10.1021/jp5052672